

## Effects of deformation microbands and twins on microstructure evolution of as-cast Mn18Cr18N austenitic stainless steel

Fengming Qin, Yajie Li, Wenwu He, Xiaodong Zhao, and Huiqin Chen<sup>a)</sup>

*School of Materials Science and Engineering, Taiyuan University of Science and Technology, Taiyuan 030024, People's Republic of China*

(Received 28 June 2017; accepted 8 September 2017)

Hot deformation behavior and microstructure evolution of as-cast Mn18Cr18N austenitic stainless steel were investigated by isothermal compression experiments. The results indicate that the microstructure evolution of the as-cast Mn18Cr18N steel is sensitive to strain rates. Discontinuous dynamic recrystallization, characterized by nucleation and growth controlled by grain boundary migration, occurs at lower strain rates. However, higher strain rates result in higher adiabatic temperature rise, which could be contributed to dynamic recrystallization (DRX) nucleation and growth by acceleration boundary migration. In addition, at higher strain rates, a large number of deformation microbands in the interior of coarse columnar grains were observed, which would provide potential nucleation sites for DRX. Meanwhile, a great number of  $\Sigma 3$  twins were observed, which reveals that twinning accelerates the separation of subgrains from bulging grain boundaries, and the iterative processing among  $\Sigma 3$  twins and its variants promotes the transformation from specific CSL grain boundaries to random high-angle boundaries.

### I. INTRODUCTION

Austenitic stainless steels with excellent properties are widely used in nuclear power industries, power plants, and medicine equipments.<sup>1,2</sup> Mn18Cr18N austenitic stainless steel with high nitrogen content, as a special kind of developed structural material used in the production of the retaining ring of power generators,<sup>3</sup> has been paid increasing attention. With the development of metallurgical technology, electro-slag re-melting (ESR) has become an attractive method used for producing consolidated, homogenized, and pure ingots of austenitic stainless steel. However, coarse grains, especially coarse columnar grains, are more prominent.<sup>4</sup> Meanwhile, the hot deformation activation energy of as-cast Mn18Cr18N steel is about 672 kJ/mol, which is higher than that of conventional austenitic stainless steel, such as 304 (426 kJ/mol) and 316LN (459 kJ/mol).<sup>5</sup> It implies that the deformation resistance for as-cast Mn18Cr18N steel is high, and the recrystallization is more difficult during hot deformation process. The cogging and forging of the ingot become key steps during the primary process of large structural forgings and play a decisive role on the performance of the large structural part.<sup>6</sup> Therefore, hot deformation parameters for the ingot cogging and forging need to be optimized, and the microstructure evolution mechanism needs to be clarified for as-cast Mn18Cr18N austenitic stainless steel.

Stress–strain curves can be used to describe the hot deformation behavior and predict the microstructure evolution to a certain extent. The hot deformation behavior of austenitic stainless steels reflects the dynamic equilibrium between work hardening and flow softening at elevated temperatures.<sup>7</sup> In addition, hot deformation results in increasing of the stored energy within the deformed material in the form of high dislocation densities, which causes work hardening. On the contrary, dynamic recovery (DRV) and dynamic recrystallization (DRX) cause a reduction in the dislocation density and flow softening in the stress–strain curve.<sup>8</sup> The DRX nucleation and growth process are often associated with the formation of  $\Sigma 3$  twins,<sup>9–11</sup> which further promote the DRX progress. That is to say, DRX is recognized as an important method to control the microstructure and properties of metallic materials.<sup>12,13</sup>

Among hot deformation parameters, the strain rate has a complex influence on the DRX kinetics.<sup>14</sup> At lower strain rates ( $<1 \text{ s}^{-1}$ ), time is enough for dislocation multiplication and migration. And dislocations tend to rearrange and form more organized sub-grains during deformation at higher temperatures. These sub-grains are easy to become DRX nuclei by grain boundary migration or merger during the following deformation process, which will result in a decrease of the critical strain for DRX.<sup>15,16</sup> Strain concentration will induce dislocation pile-up and grain boundary migration. The new nucleus of DRX will appear after the dislocation density reaches a critical value. Therefore, new DRX grains preferentially nucleate along pancaked and serrated initial grain

Contributing Editor: Jürgen Eckert

<sup>a)</sup>Address all correspondence to this author.

e-mail: chenhuiqin@tyust.edu.cn

DOI: 10.1557/jmr.2017.389

boundaries and grow until a layer of DRX grains cover the boundaries. It has been reported as a necklace structure,<sup>5,9,17,18</sup> which is generally observed at the early stage of discontinuous dynamic recrystallization (DDRX). However, at higher strain rates ( $>1 \text{ s}^{-1}$ ), DRX can be accelerated by deformation microbands, formation of  $\Sigma 3$  twins, and adiabatic heating for different materials, respectively.<sup>14,19,20</sup> For example, Favre et al.<sup>21</sup> observed the acceleration process in DRX and the second nucleation mechanism involving annealing twins at strain rates higher than  $1 \text{ s}^{-1}$ . Wang et al.<sup>10</sup> also reported that twinning plays an important role in nucleation and growth of DRX grains in the 800H alloy. In other words, acceleration of DRX by strain rates is attributed to the high accumulation rate of dislocation as well as to the adiabatic temperature rise during deformation with a higher strain rate.<sup>11</sup> In addition, Yanushkevich and his co-workers reported that deformation microbands could introduce large misorientations and promote DRX progress.<sup>20</sup> The aforementioned discussions indicate that DRX could be accelerated by both high and low strain rates, but the DRX nucleation mechanism is different. The microstructure evolution during deformation with lower strain rates has been reported by extensive studies; however, there are fewer studies on the deformation mechanism of as-cast Mn18Cr18 steel at high strain rates. Hence, clarifying the effect of high strain rates on the DRX behavior during hot deformation is very meaningful for optimizing hot deformation parameters.

In the current study, the effect of hot deformation parameters on the microstructure evolution of as-cast Mn18Cr18N austenitic stainless steel was investigated. This work was principally focused on the DRX nucleation mechanism and the role of deformation microbands and  $\Sigma 3$  twins on DRX nucleation and growth at a high strain rate.

## II. MATERIAL AND METHODS

The as-cast Mn18Cr18N austenitic stainless steel used in this investigation was manufactured by a  $\text{N}_2$  gas-pressurized electro-slag ESR. The cast ingot was supplied as a cylinder with the size of  $\Phi 300 \times 130 \text{ mm}$  and the chemical composition of the steel is listed in Table I. The initial microstructure of Mn18Cr18N ESR steel was shown in Fig. 1. The microstructure consists of abundant austenite columnar grains with a few  $\delta$  ferrites (vermicular morphology) distributing at the grain boundaries. The formation of the special microstructure

may be due to the directional heat transfer during the ESR process.

Cylindrical isothermal compression samples with the size of  $\Phi 8 \times 12 \text{ mm}$  were machined from the as-cast ingot. The axes of the specimens parallel to the columnar grain axes are roughly perpendicular to the axes of ingots. The samples were subjected to isothermal compression tests on a Thermecmaster-Z thermal-mechanical modeling system at deformation temperatures of 950–1200 °C and strains of 0.35–0.69 with strain rates of 0.001–10  $\text{s}^{-1}$ . To minimize the friction, graphite foil in combination with high-temperature lubricants ( $\text{MoS}_2$ ) was used. Therefore, the barreling was almost not observed in this study. The samples were heated to the deformation temperature at the rate of 10 °C/s and held for 120 s for soaking. After isothermal compression, the compressed specimens were quenched immediately to room temperature with 50 °C/s using liquid nitrogen to freeze the high-temperature microstructure.

The isothermally compressed samples were sectioned along its central axis. The metallographic samples were prepared by following standard metallographic procedures. The metallographic samples were etched with a mixture reagent (1 mL HF, 1.5 mL HCl, 2.5 mL  $\text{HNO}_3$ , and 95 mL  $\text{H}_2\text{O}$ ) for about 120 s at room temperature, and a microstructural analysis was conducted on a Zeiss optical microscope. The samples for electron backscatter diffraction (EBSD) were electrolytic polished using 4 vol% perchloric acid-96 vol% alcohol solution at 40 V for 30 s at room temperature. EBSD testing was carried out using a ZEISS ULTRA 55 field-emission scanning electron microscope (Carl Zeiss AG, Oberkochen, Germany). The step size in EBSD scan was 0.5–0.8  $\mu\text{m}$ . HKL Channel 5 software (Oxford Instruments, Abingdon, United Kingdom) was used to analyze the EBSD scan data. The thin foils for transmission electron microscope (TEM) were electro-polished in a 5 vol% perchloric acid and in a 95 vol% acetic acid mixture at 25 V and 30 mA at room temperature. TEM analysis was conducted on a Tecnai F30 G2 microscope at 300 kV (FEI, Hillsboro, Oregon).

## III. RESULTS

### A. Flow behavior

The true stress–strain curves can be used to analyse the mechanism of hot deformation behavior at different deformation conditions. The true stress–strain curves of as-cast Mn18Cr18N austenitic stainless steel at different deformation temperatures and strain rates were shown in

TABLE I. Chemical composition (in wt%) of Mn18Cr18N steel.

Cr	Mn	Ni	Mo	Cu	Si	Al	C	Ti	N	P	S
20	19.21	0.14	0.022	0.035	0.59	0.023	0.074	0.016	0.61	0.014	0.001

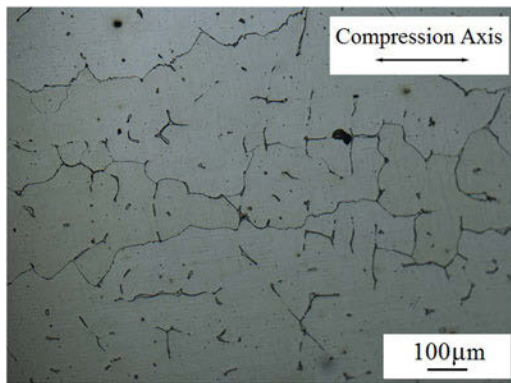


FIG. 1. The initial microstructure of as-cast Mn18Cr18N steel.

Fig. 2. The peak stress increased with decreasing of the temperature and the increasing of the strain rate. At the constant temperature, the flow behavior varies with the strain rate. When the strain rate is lower, the curves are characterized by softening after peak stresses, which is often caused by DRX. However, the softening rate decreased with the increasing of strain rates due to the short time for DRV. When the balance between strain hardening and DRV is reached, the curves keep constant after peak stresses. When the strain rate increased at a certain value, the adiabatic temperature rise needs to be considered, which can cause softening again.

(i) At lower strain rates ( $0.001\text{--}0.01\text{ s}^{-1}$ ), the flow stress roughly decreased with the increasing of the strain. However, of particular interest is the observation that the true stress–strain curves at higher deformation temperatures ( $1100$  and  $1200\text{ }^{\circ}\text{C}$ ) show a steady flow characteristic after the peak value. It is because that the stress easily reaches to a steady value at an early stage of deformation at the higher temperature and lower strain rate. It has been reported that the high temperature promotes the diffusion of atoms, and low strain rates provide full time to grow up.<sup>22</sup> As a result, at a strain rate of  $0.001\text{ s}^{-1}$ , the steady state is achieved at  $1100\text{ }^{\circ}\text{C}$ ; but at a strain rate of  $0.01\text{ s}^{-1}$ , the steady state is achieved at  $1200\text{ }^{\circ}\text{C}$ .

(ii) At a medium strain rate of  $0.1\text{ s}^{-1}$ , the true stress–strain curves reveal typical DRX characteristics and a continuous flow softening behavior at all the examined temperatures. However, a detailed microstructural analysis is required to decide the flow softening mechanism.

(iii) At higher strain rates ( $1\text{--}10\text{ s}^{-1}$ ), the true stress–strain curves clarify different characteristics. At a strain rate of  $1\text{ s}^{-1}$ , the flow stress increased continuously with the increasing of strain, which indicates that work hardening is predominant during deformation as seen in Figs. 2(a)–2(c). However, work hardening was not obvious at a deformation temperature of  $1200\text{ }^{\circ}\text{C}$  [as shown in Fig. 2(d)]. It is because that the flow softening is accelerated at a higher deformation temperature. When

the strain rate was increased to  $10\text{ s}^{-1}$ , the stress–strain curves reveal typical DRX characteristics, and the flow stress decreased after the peak stress, which indicated that a certain degree of flow softening reappeared at a high strain rate. The flow softening may be associated with the temperature rise and DRX behavior.<sup>23</sup>

In short, the true stress–strain curves reveal a particular flow feature compared to the common flow behavior, and further analysis is necessary to decide the flow softening mechanism.

## B. Effect of strain rates on microstructure evolution

Figure 3 shows the color IPF maps of samples deformed to 0.69 at  $950\text{ }^{\circ}\text{C}$  with different strain rates. IPF maps indicate that nucleation, growth, and the DRX grain size of Mn18Cr18N steel during deformation are strongly influenced by strain rates. Firstly, at lower strain rates ( $0.001\text{--}0.01\text{ s}^{-1}$ ), DRX grains formed a necklace structure along the original grain boundaries,<sup>9</sup> as shown in Figs. 3(a) and 3(b). In addition, the recrystallization fraction and grain size increased with the decreasing of strain rates, which is consistent with that of the conventional DDRX. The acceleration of DRX with the decreasing of strain rates is mainly due to the longer deformation time for nucleation and growth of DRX grains.<sup>11</sup> Then, at a medium strain rate of  $0.1\text{ s}^{-1}$ , the recrystallization fraction increased to 32%, while the DRX grain size also increased [Fig. 3(c)], which is an abnormal phenomenon. Meanwhile, it should be emphasized that a number of deformation microbands occurred inside the deformed parent grains. However, at the higher strain rates ( $1\text{--}10\text{ s}^{-1}$ ), the recrystallization fraction increased with the increasing of strain rates. At a strain rate of  $1\text{ s}^{-1}$ , DRX grains were almost absent, and a large number of deformation microbands occupied the deformed columnar grain, which is very possible that a shorter time is not enough for DRX. When the strain rate increased to  $10\text{ s}^{-1}$ , DRX grains reappeared, and the fraction of DRX increased to 26.6%. In this case, it is very possible that DRX grains nucleate within the deformation microbands without the necklace structure. It indicates that the microstructure evolution mechanism is different at low and high strain rates. DRX is mainly influenced by deformation time at a lower strain rate, while DRX may be accelerated by deformation microbands at a higher strain rate. However deformation with a medium strain rate of  $0.1\text{ s}^{-1}$  may be a transitional stage. As a result, further analysis is necessary to confirm the role of deformation microbands on DRX during hot deformation with higher strain rates.

The samples were compressed to different strains at a constant temperature of  $1000\text{ }^{\circ}\text{C}$  with a higher strain rate of  $1\text{ s}^{-1}$ , and its EBSD grain boundary maps were

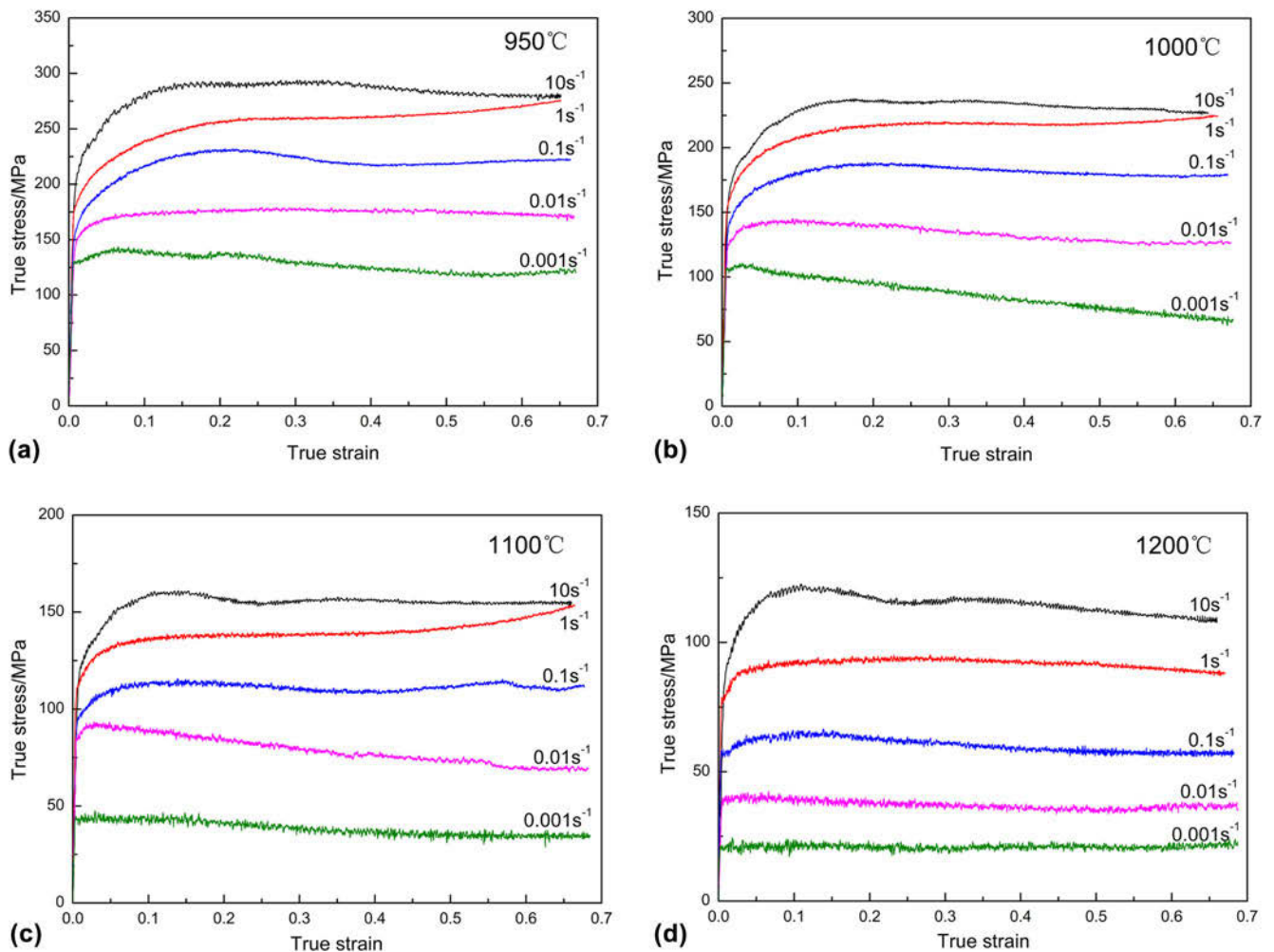


FIG. 2. The true stress-true strain curves at different temperatures and strain rates (a) 950 °C, (b) 1000 °C, (c) 1100 °C, and (d) 1200 °C.

shown in Fig. 4. The original columnar grains were segmented via a large number of deformation microbands, as shown in Fig. 4(a). A few low-angle boundaries (LABs) were randomly distributed inside the banded structure, and there were almost no recrystallized grains, which is attributed to the lower deformation-stored energy at a strain of 0.35. As the strain increased to 0.51, higher-density LABs were clustered within the deformation bands, and DRX was initiated [Fig. 4(b)]. With strain increasing to 0.69, abundant DRX grains formed by consuming the deformed structures [Fig. 4(c)]. As expected, the microstructure evolution of the samples at the higher strain rates is associated with the deformation microbands. Another interesting point is that a majority of DRX grains are  $\Sigma 3$  twins. It is very possible that DRX in this case is also related with the twinning during hot deformation. The strain effect on the distribution of the boundary misorientation was shown in Fig. 4(d), which indicates moderate transition from LABs to HABs. With

the increasing of strain, the fraction of LABs gradually decreased, and the HABs correspondingly increased from 4.45% ( $\epsilon = 0.35$ ) to 15.72% ( $\epsilon = 0.69$ ). It is because that the high strain causes an increase of the deformation-stored energy, which promotes the DRX progress.

EBSD maps of the samples compressed to 0.69 at different deformation temperatures with a higher strain rate of  $1 \text{ s}^{-1}$  were shown in Fig. 5. There was a significant increase of the DRX fraction as well as the DRX grain size with increasing of the deformation temperature. And the almost full recrystallization was obtained at the deformation temperature of 1200 °C. In addition, Fig. 5(d) indicates that a variation of the  $\Sigma 3$  twin fraction (length ratio in the boundary misorientation distribution map obtained from the EBSD observation) with the deformation temperature is roughly in accordance with DRX grains. It is very possible that twinning promotes the recrystallization progress during plastic deformation at higher strain rates.



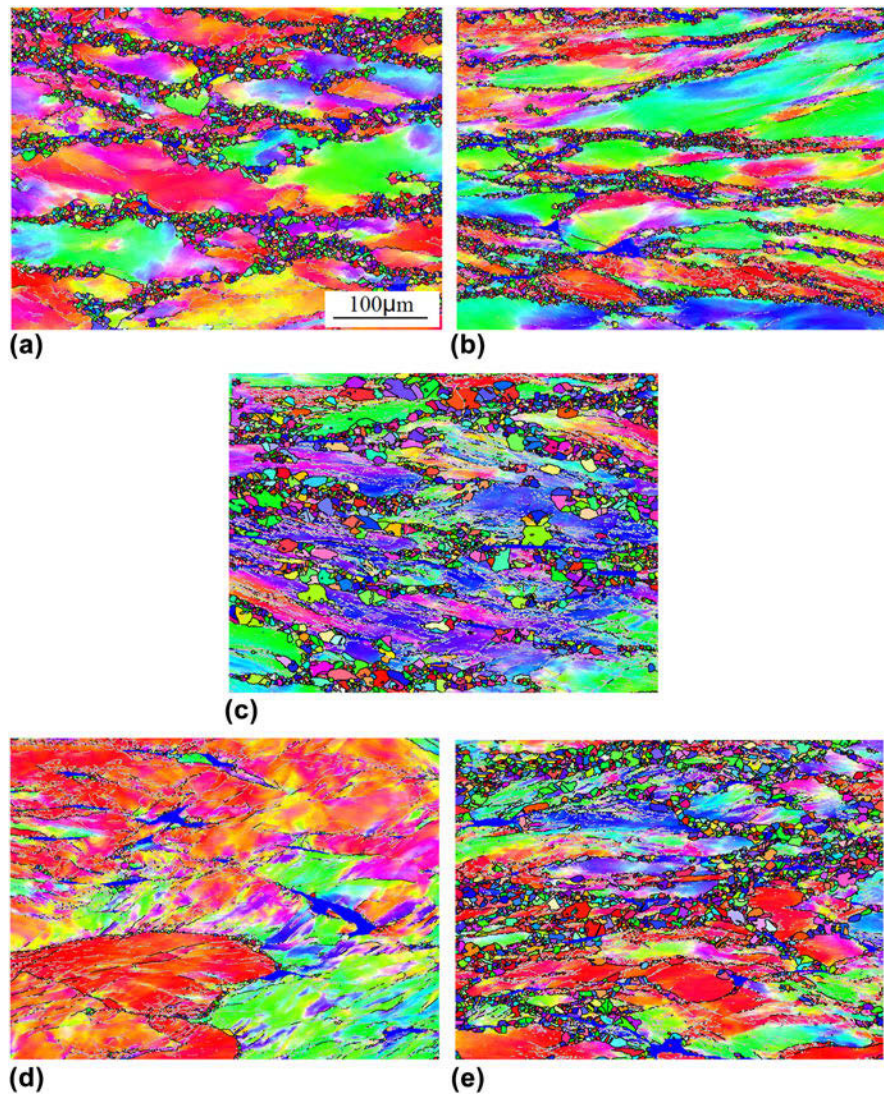


FIG. 3. Color IPF maps of the compressed samples at 950 °C and different strain rates of (a) 0.001 s<sup>-1</sup>, (b) 0.01 s<sup>-1</sup>, (c) 0.1 s<sup>-1</sup>, (d) 1 s<sup>-1</sup>, and (e) 10 s<sup>-1</sup> ( $\delta$  ferrites-blue, 5–15°-silver, >15°-black).

#### IV. DISCUSSION

##### A. Adiabatic temperature rise

Deformation heating is pronounced at a higher strain rate, which has been reported in a nickel-based super alloy,<sup>24</sup> TC21 titanium alloy,<sup>6</sup> and 316L(N) austenitic stainless steel.<sup>14</sup> It is extremely likely that the adiabatic temperature rise ( $\Delta T$ ) accelerated flow softening at a higher strain rate. That is because that the adiabatic temperature rise may have some influence on the recrystallization kinetics. During hot deformation process with higher strain rates, a large amount of plastic deformation energy is converted into heat, which can cause material temperature rise in a short time. As a result, it accelerates the recrystallization process. The amount of adiabatic temperature rise could be calculated according to the following equation<sup>25</sup>:

$$\Delta T = \frac{0.95\eta}{\rho C_p} \int_0^\varepsilon \sigma d\varepsilon \quad , \quad (1)$$

Where  $\rho$  is the density of the deformed material (7.586 g/cm<sup>3</sup>),  $C_p$  is the specific heat [0.5 J/(g K)],  $\sigma$  is the true flow stress,  $\varepsilon$  is the true strain, and  $\eta$  is the thermal efficiency, which can be calculated according to the following equations<sup>26</sup>:

$$\eta = \begin{cases} 0 & \dot{\varepsilon} \leq 0.001 \text{ s}^{-1} \\ 0.316 \log \dot{\varepsilon} + 0.95 & 0.001 \text{ s}^{-1} < \dot{\varepsilon} < 1 \text{ s}^{-1} \\ 0.95 & \dot{\varepsilon} \geq 1 \text{ s}^{-1} \end{cases} \quad . \quad (2)$$

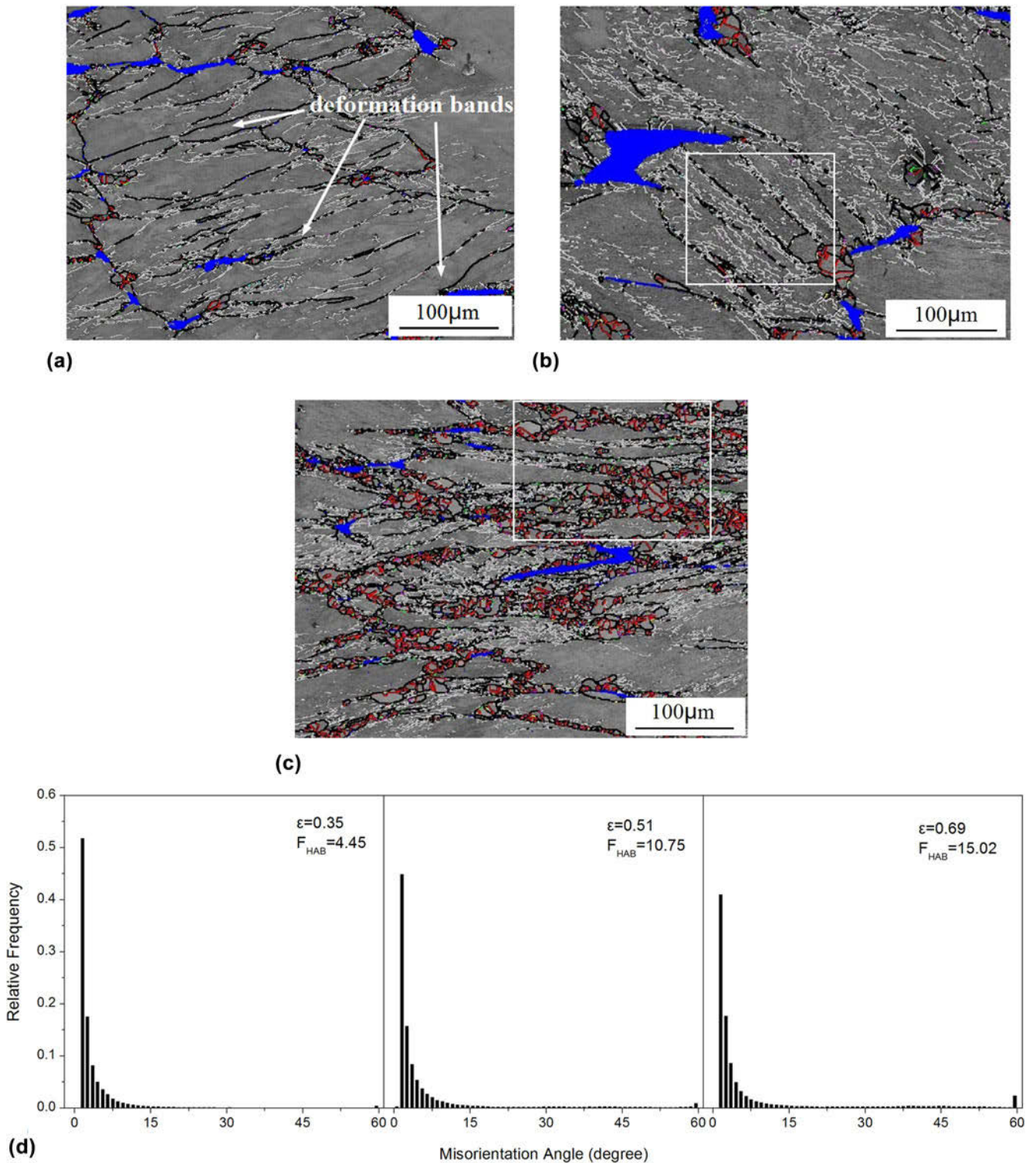


FIG. 4. EBSD grain boundary maps of the compressed samples at 1000 °C, the strain rate of  $1 \text{ s}^{-1}$  and the strains of (a) 0.35, (b) 0.51, (c) 0.69 and (d) corresponding grain boundary misorientation distributions ( $\delta$  ferrites-blue, 5–15°-silver, >15°-black,  $\Sigma 3$ -red,  $\Sigma 9$ -green, and  $\Sigma 27$ -purple).

Figure 6 shows the temperature rise as a function of the deformation temperature and strain rate under a strain of 0.69. It can be seen that  $\Delta T$  increases with the increasing of the strain rate and the decreasing of the deformation

temperature. However, the temperature rise is more sensitive to the strain rate, and it can be above 30 °C at the strain rate higher than  $1 \text{ s}^{-1}$  and at the deformation temperature lower than 1050 °C. A higher  $\Delta T$  could be



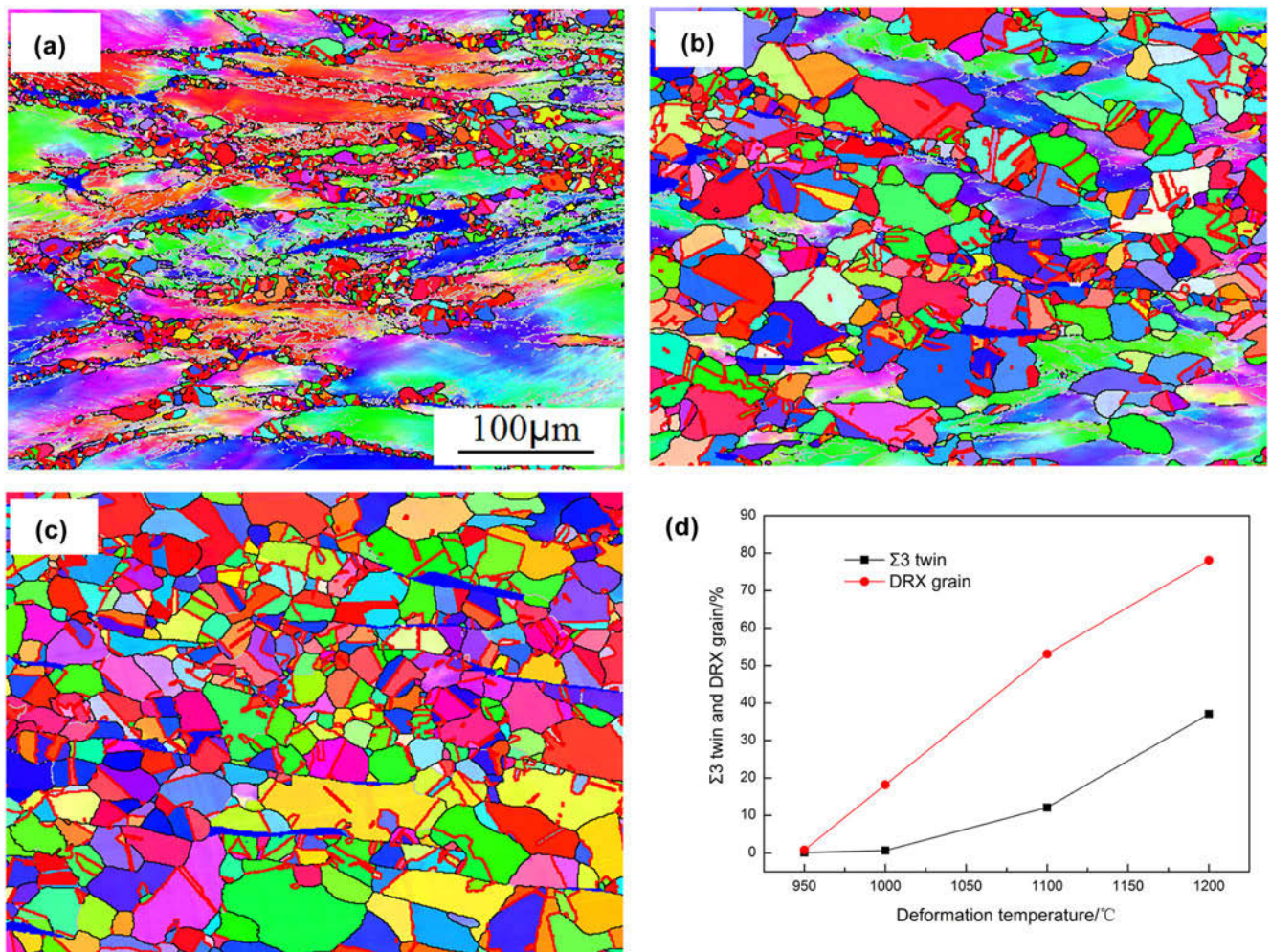


FIG. 5. Color IPF maps of the compressed samples at a strain of 0.69, a strain rate of  $1 \text{ s}^{-1}$  and the temperatures of (a) 1000 °C, (b) 1100 °C, (c) 1200 °C, and (d) the fraction of  $\Sigma 3$  twins and DRX grains ( $\delta$  ferrites-blue, 5–15°-silver, >15°-black, and  $\Sigma 3$ -red).

contributed to DRX nucleation and grain boundary migration, which has been reported in Mg and Cu alloys.<sup>19,27</sup> Therefore, it suggested that the adiabatic temperature rise also plays an important role in the flow softening behavior of Mn18Cr18N austenitic stainless steel.

## B. Deformation microbands

As aforesaid in Sec. III.B, a large number of deformation bands were observed inside deformed parent grains at a higher strain rate. To clarify the effect of deformation microbands on the recrystallization mechanism at higher strain rates, partial high-resolution EBSD maps of samples deformed at 1000 °C and TEM micrographs of the sample deformed at 1000 °C were shown in Fig. 7. The results indicate that the grain refinement process in the interior of the as-cast columnar parent grains may be divided into two stages, i.e., the formation of deformation microbands and DRX grains nucleation and progress.

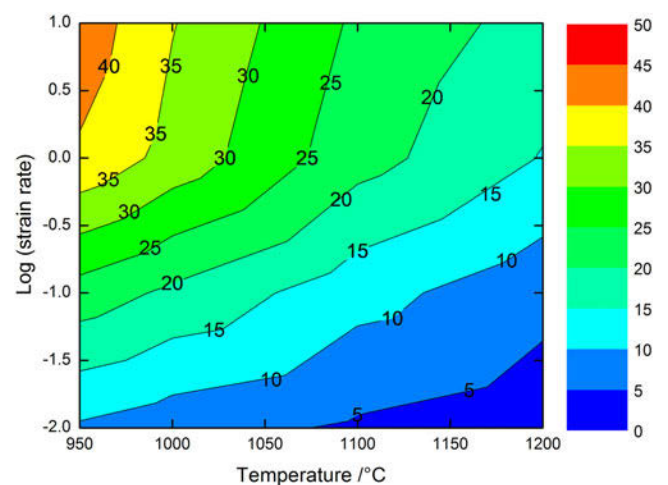


FIG. 6. The temperature rise contour plot at a strain of 0.69 as a function of the compression temperature and strain rate.

Stage I: In the primary stage of deformation, the columnar grain is segmented by roughly parallel deformation bands due to the nonuniform plastic

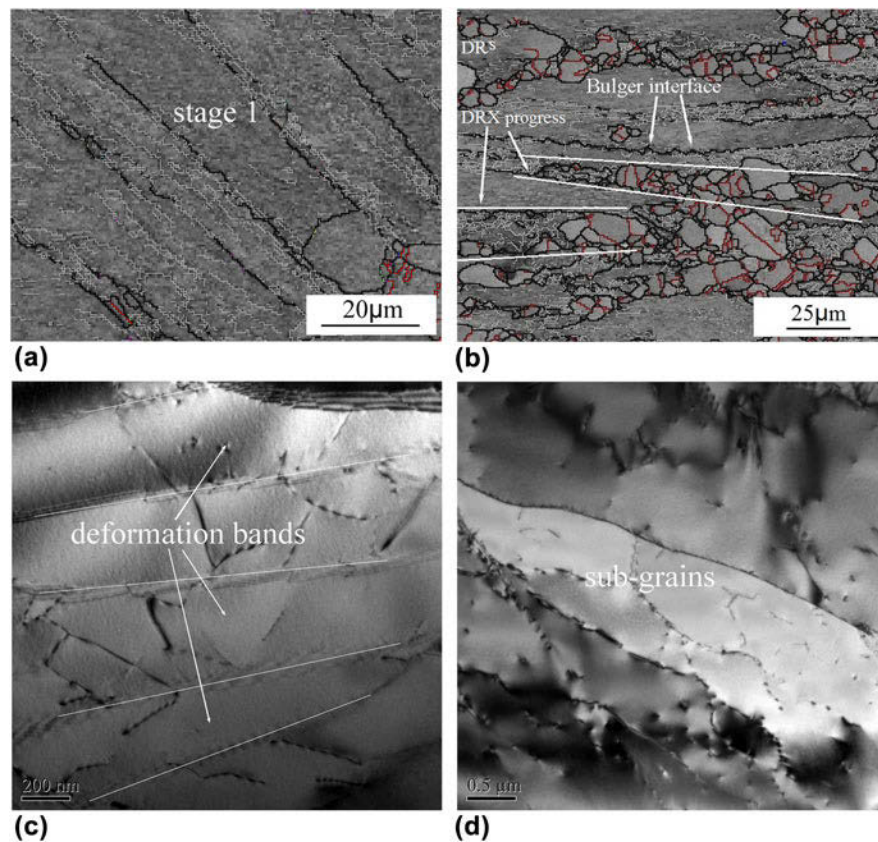


FIG. 7. EBSD maps of the deformed sample at 1000 °C and the strain rate of  $1 \text{ s}^{-1}$  (a) and (b) partially enlarged detail in Figs. 4(b) and 4(c), respectively; corresponding TEM micrographs of (c) deformation microbands and (d) nucleation inside deformation microbands.

deformation at higher strain rates [Fig. 7(a)], which is in line with the study reported by Yanushkevich et al.<sup>20</sup> Moreover, HABs occurred in the regions with sufficient deformation-stored energy, while LABs occurred in the regions with a lower strain concentration. There is only the evolution of substructures without the appearance of pronounced recrystallization grains, which indicates that stage I is the incubation period of the microstructure evolution. Of particular interest is that the LABs in the interior of the deformation bands are also roughly parallel to the HABs. It is very possible that those parallel LABs could transform into the HABs, resulting in the formation of thin deformation microbands.

Stage II: When the strain increased to 0.69, recrystallization is activated due to the high deformation-stored energy and strain concentration. The nucleation of DRX grains and progress are revealed in Fig. 7(b). The bulging of the interface between deformation microbands is frequently observed at the early stage of hot deformation. Then, recrystallization nuclei form in the serrated region due to plastic deformation accumulation inside the deformation microbands, and recrystallized grains are separated from the bulged portions with increasing the strain gradient. That is to say, the microstructure fragmentation is related with deformation microbands, which

is consistent with previous reports.<sup>28,29</sup> Because of the coarse columnar grains and the fewer grain boundaries of as-cast Mn18Cr18N austenitic stainless steel, the interfaces (with high angle misorientations) between the deformation microbands as the initial grain boundary provide a preferential nucleation site and accelerate the recrystallization progress. Meanwhile, the significant increasing of the fraction of DRX grains can also be seen in Fig. 7(b), which is the development stage of recrystallization. It should be emphasized that abundant recrystallized grains are observed inside the deformation microbands [as shown by the roughly parallel white lines in Fig. 7(b)]. This progress is characterized by bulging of the grain boundary and transformation from LABs to HABs, which reveal that the mechanism of grain refinement at higher rates is related with CDRX and DDRX. Meanwhile, substantial deformation microbands can also be observed in TEM micrographs in Fig. 7(c), and a few sub-grains formed in the interior of deformation bands can be observed in [Fig. 7(d)]. This conclusion coincides with the results obtained by EBSD.

In addition, a large number of  $\Sigma 3$  twins occurred in recrystallized regions [Fig. 7(b)], which indicate that DRX may be associated with twinning. Several researchers reported that the increasing of  $\Sigma 3$  twins



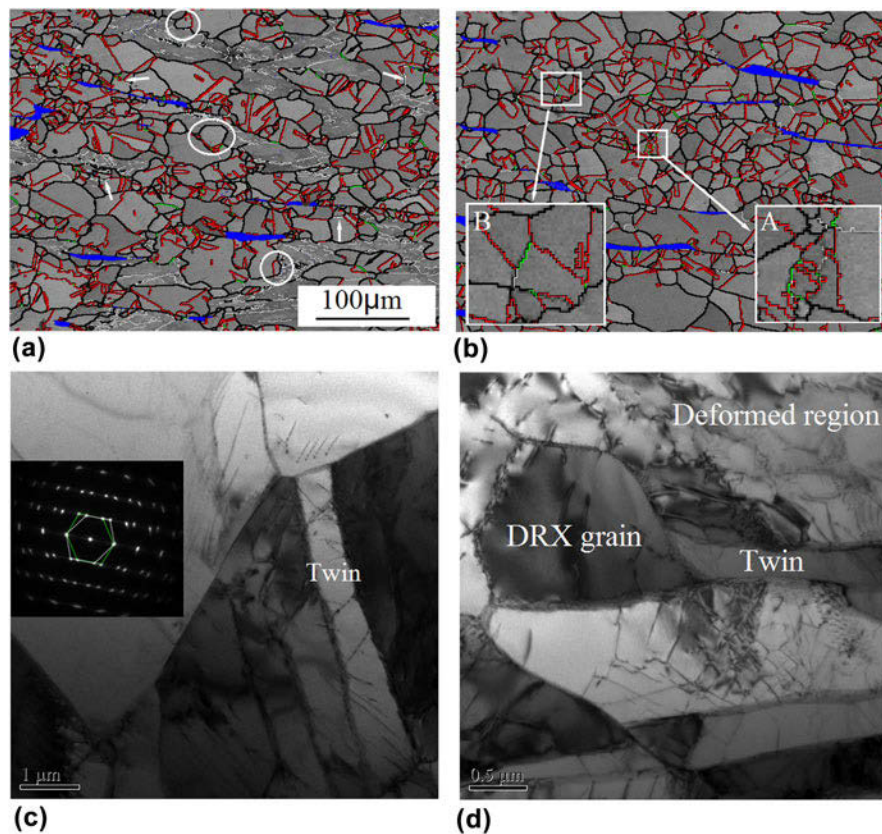


FIG. 8. EBSD grain boundary maps of samples compressed to 0.69 with a strain rate of  $1 \text{ s}^{-1}$  at different temperatures (a) 1100 °C, (b) 1200 °C; (c) and (d) indicate TEM micrographs of (a) and (b) ( $\delta$  ferrites-blue,  $5\text{--}15^\circ$ -silver,  $>15^\circ$ -black,  $\Sigma 3$ -red,  $\Sigma 9$ -green, and  $\Sigma 27$ -white).

during hot deformation in materials with low SFE is attributed to the interaction between preexisting  $\Sigma 3$  boundaries or the “growth accident” of recrystallized nuclei.<sup>30–32</sup> However, in case of the as-cast Mn18Cr18N steel, the  $\Sigma 3$  twin is not observed in the initial microstructure. It was also demonstrated in our previous study that twinning accelerated the separation of subgrains from bulging preexisting grain boundaries.<sup>5</sup> As a result, the  $\Sigma 3$  twin is probably nucleated by “growth accident” of the recrystallized grains. It will be discussed how twinning promotes the recrystallization in following section.

### C. Twinning

In this study, a large number of twins are observed inside deformation micro-bands. Previous studies have reported the role of twinning on DRX and microstructure evolution in austenitic stainless steel during hot deformation with higher strain rates.<sup>11</sup> It is generally recognized that deformation is coordinated by the migration of high-angle boundaries.<sup>33,34</sup> Taking into account as-cast Mn18Cr18N with fewer grains in the observed field, it is hard to see the migration of abundant grain boundaries. Meanwhile, it has been reported that a cross slip is inhibited for metals with low value of SFE.<sup>8</sup> As-cast

Mn18Cr18N steel is of a low SFE of  $24 \text{ mJ/m}^2$ , which has been reported by our previous study.<sup>5</sup> Low SFE promotes the formation of twins due to the lower twin boundary interfacial energy.<sup>11</sup> Therefore, twinning is favored for this material during the deformation at higher strain rates.

A great number of  $\Sigma 3$  twins and a few  $\Sigma 9$ ,  $\Sigma 27$  boundaries were observed in the recrystallized region deformed to 0.69 at 1100 °C with a strain rate of  $1 \text{ s}^{-1}$  [Fig. 8(a)]. When the deformation temperature rose up to 1200 °C [Fig. 8(b)], the fraction of recrystallized grains increased by means of consuming the deformed substructure compared to Fig. 8(a). Of particular interest is that the majority of  $\Sigma 3$  twins is formed in the interior of the recrystallized grains, as shown in Figs. 8(a) and 8(b). The  $\Sigma 3$  coherent twins with a misorientation angle less than  $1.7^\circ$  away from the ideal  $\langle 111 \rangle$   $60^\circ$  misorientation is usually identified as primary twins, which is characterized by a straight and a parallel boundary. The  $\Sigma 3$  twins occurred at bulging boundaries inducing the separation of recrystallized grains from parent grains, as shown by circles in Fig. 8(a). It is possible that the  $\Sigma 3$  twin may improve the DRX progress by a separation mechanism. Meanwhile,  $\Sigma 9$  and  $\Sigma 27$  are called as secondary twins, which are produced by the interaction of  $\Sigma 3$  boundaries.

The iterative processing among  $\Sigma 3$  and its variants is complicated; however, this process always follows the relationship:  $\Sigma 3^n + \Sigma 3^{n+1} = \Sigma 3$  or  $\Sigma 3^n + \Sigma 3^{n+1} = \Sigma 3^{n+2}$ .<sup>30,35,36</sup> Other CSL grain boundaries ( $\Sigma 9$  and  $\Sigma 27$ ) have deviated from the morphology of coherent twins and will transform to random high-angle boundaries, as shown by black and white arrows in Fig. 8(a), respectively. The iterative processing among CSL grain boundaries can be seen in the enlarged region in Fig. 8(b). Region A shows that a few  $\Sigma 9$  boundaries (green) distribute in the enrichment area of  $\Sigma 3$  coherent boundaries (red), which may indicate that the interaction between two  $\Sigma 3$  coherent boundaries form a  $\Sigma 9$  boundary. The triple junction comprising of  $\Sigma 3$ ,  $\Sigma 9$ , and  $\Sigma 27$  (white) was observed in Region B. It is very possible that  $\Sigma 27$  is formed by the interaction between  $\Sigma 3$  and  $\Sigma 9$ . That is to say, formation of secondary twins is considered as a transition stage from deformed parent grains to recrystallized equiaxed grains. Twins are also observed in TEM micrographs in Figs. 8(c) and 8(d), which may be formed by the growth accidents during the DRX process. Figure 8(d) indicates that a recrystallized equiaxed grain adjacent to the twin occurred without high dislocation density. Combining with the recrystallized grain, the twin boundary may transform into a random high-angle grain boundary. This process is accompanied with the migration of the grain boundary and consumption of surrounding dislocations. In summary, twinning is an indispensable procedure of DRX and distinctly accelerates its progress.

## V. CONCLUSIONS

The DRX behavior of as-cast Mn18Cr18N austenitic stainless steel with the coarse columnar grain structure was studied in the strain rate range of 0.001–10 s<sup>-1</sup> at 950–1200 °C through isothermal compression experiments. The conclusions can be drawn as follows:

(1) Microstructure evolution of as-cast Mn18Cr18N steel during hot deformation is sensitive to the strain rate. At lower strain rates (0.001–0.01 s<sup>-1</sup>), DRX grains formed a necklace structure along the original grain boundaries, and a fraction of DRX grains and grain size increase with the decreasing of strain rates, which is consistent with that of the conventional DDRX.

(2) At a strain rate of 1 s<sup>-1</sup>, the true stress–strain curves indicate that the obvious flow softening only occurred at 1200 °C. However, the flow curves at a strain rate of 10 s<sup>-1</sup> exhibit significant stress softening at temperatures from 950 °C to 1200 °C. The acceleration of DRX at higher strain rates is due to the adiabatic temperature rise ( $\Delta T$ ), deformation microbands, and annealing twins.

(3) Adiabatic temperature rise ( $\Delta T$ ) increases with increasing the strain rate and decreasing the deformation

temperature. It can be above 30 °C at the strain rate higher than 1 s<sup>-1</sup> and at the deformation temperature lower than 1050 °C.

(4) A large number of deformation microbands were observed in the interior of the deformed columnar grains at higher strain rates. The interfaces between deformation microbands can serve as preferential nucleation sites for DRX, which is similar to the original high-angle grain boundaries.

(5) The variation of  $\Sigma 3$  twin fraction with the deformation temperature is roughly in accordance with the DRX grains. Twinning plays a significant role on DRX progress. On one hand, the  $\Sigma 3$  twin may accelerate the DRX process by separation mechanism. On the other hand, the iterative among the  $\Sigma 3$  and its variants can promote the transformation from CSL grain boundaries to random high-angle boundaries.

## ACKNOWLEDGMENT

This work was financially supported by the National Natural Science Foundation of China (No. 51575372).

## REFERENCES

1. H.Y. Sun, Y.D. Sun, and R.Q. Zhang: Hot deformation behavior and microstructural evolution of a modified 310 austenitic steel. *Mater. Des.* **64**, 374 (2014).
2. Y.H. Zhou, C.X. Liu, Y.C. Liu, Q.Y. Guo, and H.J. Li: Coarsening behavior of MX carbonitrides in type 347H heat-resistant austenitic steel during thermal aging. *Int. J. Miner., Metall. Mater.* **23**, 283 (2016).
3. F. Li, H.Y. Zhang, W.W. He, H.Q. Chen, and H.G. Guo: Compression and tensile consecutive deformation behavior of Mn18Cr18N austenite stainless steel. *Acta Metall. Sin.* **52**, 956 (2016).
4. M. Kermajani, S. Raygan, K. Hanayi, and H. Ghaffari: Influence of thermomechanical treatment on microstructure and properties of electroslag remelted Cu–Cr–Zr alloy. *Mater. Des.* **51**, 688 (2013).
5. F.M. Qin, H. Zhu, Z.X. Wang, X.D. Zhao, W.W. He, and H.Q. Chen: Dislocation and twinning mechanisms for dynamic recrystallization of as-cast Mn18Cr18N steel. *Mater. Sci. Eng., A* **684**, 634 (2017).
6. Y.C. Zhu, W.D. Zeng, J.L. Liu, Y.Q. Zhao, Y.G. Zhou, and H.Q. Yu: Effect of processing parameters on the hot deformation behavior of as-cast TC21 titanium alloy. *Mater. Des.* **33**, 264 (2012).
7. J.Q. Zhang, H.S. Di, and X.Y. Wang: Flow softening of 253MA austenitic stainless steel during hot compression at higher strain rates. *Mater. Sci. Eng., A* **650**, 483 (2016).
8. F.J. Humphreys and M. Hatherly: *Recrystallization and Related Annealing Phenomena* (Elsevier Ltd., Oxford, U.K., 2004).
9. D. Ponge and G. Gottstein: Necklace formation during dynamic recrystallization: Mechanisms and impact on flow behavior. *Acta Mater.* **46**, 69 (1998).
10. X. Wang, E. Brunger, and G. Gottstein: The role of twinning during dynamic recrystallization in alloy 800H. *Scr. Mater.* **46**, 875 (2002).
11. S. Mandal, A.K. Bhaduri, and V.S. Sarma: Role of twinning on dynamic recrystallization and microstructure during moderate to high strain rate hot deformation of a Ti-modified austenitic stainless steel. *Metall. Mater. Trans. A* **43**, 2056 (2012).

12. S.S. Satheesh-Kumar, M. Vasanth, V. Singh, P. Ghosal, and T. Raghu: An investigation of microstructural evolution in 304L austenitic stainless steel warm deformed by cyclic channel die compression. *J. Alloys Compd.* **699**, 1036 (2017).
13. Y.M. Li, Y.C. Liu, C.X. Liu, C. Li, Y. Huang, H.J. Li, and W.Y. Li: Carbide dissolution and precipitation in cold-rolled type 347H austenitic heat-resistant steel. *Mater. Lett.* **189**, 70 (2017).
14. S. Mandal, M. Jayalakshmi, A.K. Bhaduri, and V.S. Sarma: Effect of strain rate on the dynamic recrystallization behavior in a nitrogen-enhanced 316L(N). *Metall. Mater. Trans. A* **45**, 5645 (2014).
15. Q.M. Guo, D.F. Li, H.J. Peng, S.L. Guo, J. Hu, and P. Du: Nucleation mechanisms of dynamic recrystallization in Inconel 625 superalloy deformed with different strain rates. *Rare Met.* **31**, 215 (2012).
16. Y. Wang, W.Z. Shao, L. Zhen, L. Yang, and X.M. Zhang: Flow behavior and microstructures of superalloy 718 during high temperature deformation. *Mater. Sci. Eng., A* **497**, 479 (2008).
17. A. Belyakov, H. Miura, and T. Sakai: Dynamic recrystallization under warm deformation of a 304 type austenitic stainless steel. *Mater. Sci. Eng., A* **255**, 139 (1998).
18. M. El Wahabi, L. Gavard, F. Montheillet, J.M. Cabrera, and J.M. Prado: Effect of initial grain size on dynamic recrystallization in high purity austenitic stainless steels. *Acta Mater.* **53**, 4605 (2005).
19. H.Q. Sun, Y.N. Shi, M.X. Zhang, and K. Lu: Plastic strain-induced grain refinement in the nanometer scale in a Mg alloy. *Acta Mater.* **55**, 975 (2007).
20. Z. Yanushkevich, A. Belyakov, and R. Kaibyshev: Microstructural evolution of a 304-type austenitic stainless steel during rolling at temperatures of 773–1273 K. *Acta Mater.* **82**, 244 (2015).
21. J. Favre, Y. Koizumi, A. Chiba, D. Fabregue, and E. Maire: Deformation behavior and dynamic recrystallization of biomedical Co–Cr–W–Ni (L-605) alloy. *Metall. Mater. Trans. A* **44**, 2819 (2013).
22. Y.H. Zhou, Y.C. Liu, X.S. Zhou, C.X. Liu, L.M. Yu, and C. Li: Processing maps and microstructural evolution of the type 347H austenitic heat-resistant stainless steel. *J. Mater. Res.* **30**, 2090 (2015).
23. T. Seshacharyulu, S.C. Medeiros, W.G. Frazier, and Y.V.R.K. Prasad: Hot working of commercial Ti–6Al–4V with an equiaxed  $\alpha$ – $\beta$  microstructure: Materials modeling considerations. *Mater. Sci. Eng., A* **284**, 184 (2000).
24. H.B. Zhang, K.F. Zhang, H.P. Zhou, Z. Lu, C.H. Zhao, and X.L. Yang: Effect of strain rate on microstructure evolution of a nickel-based superalloy during hot deformation. *Mater. Des.* **80**, 51 (2015).
25. R.L. Goetz and S.L. Semiatin: The adiabatic correction factor for deformation heating during the uniaxial compression test. *J. Mater. Eng. Perform.* **10**, 710 (2001).
26. M. Mataya and V. Sackschewsky: Effect of internal heating during hot compression on the stress-strain behavior of alloy 304L. *Metall. Mater. Trans. A* **25**, 2737 (1994).
27. U. Andrade, M.A. Meyers, K.S. Vecchio, and A.H. Chokshi: Dynamic recrystallization in high-strain, high-strain-rate plastic deformation of copper. *Acta Metall. Mater.* **42**, 3183 (1994).
28. S.L. Wang, M.X. Zhang, H.C. Wu, and B. Yang: Study on the dynamic recrystallization model and mechanism of nuclear grade 316LN austenitic stainless steel. *Mater. Charact.* **118**, 92 (2016).
29. Q.Y. Yu, Z.H. Yao, and J.X. Dong: Deformation and recrystallization behavior of a coarse-grain, nickel-base superalloy Udimet 720Li ingot material. *Mater. Charact.* **107**, 398 (2015).
30. G. Owen and V. Randle: On the role of iterative processing in grain boundary engineering. *Scr. Mater.* **55**, 959 (2006).
31. H. Gleiter: The formation of annealing twins. *Acta Metall.* **17**, 1421 (1969).
32. S. Mahajan, C.S. Pande, M.A. Imam, and B.B. Rath: Formation of annealing twins in f.c.c. crystals. *Acta Mater.* **45**, 2633 (1997).
33. S.V. Bobylev and I.A. Ovid'ko: Stress-driven migration, convergence and splitting transformations of grain boundaries in nanomaterials. *Acta Mater.* **124**, 333 (2017).
34. C. Xie, Y.N. Wang, Q.H. Fang, T.F. Ma, and A.B. Zhang: Effects of cooperative grain boundary sliding and migration on the particle cracking of fine-grained magnesium alloys. *J. Alloys Compd.* **704**, 641 (2017).
35. L.C. Lim and R. Raj: On the distribution of  $\Sigma$  for grain boundaries in polycrystalline nickel prepared by strain annealing technique. *Acta Metall.* **32**, 1177 (1984).
36. S. Mandal, P.V. Sivaprasad, B. Raj, and V.S. Sarma: Grain boundary microstructural control through thermomechanical processing in a titanium-modified austenitic stainless steel. *Metall. Mater. Trans. A* **39**, 3298 (2008).